

PACS numbers: 52.38.Mf; 81.07.–b; 81.16.Mk
DOI: 10.1070/QE2010v040n11ABEH014446

Laser synthesis and modification of composite nanoparticles in liquids

N.V. Tarasenko, A.V. Butsen

Abstract. **The works devoted to the formation and modification of nanoparticles using laser ablation of solid targets in liquids are reviewed. Several approaches to implement laser ablation in liquids, aimed at synthesising nanoparticles of complex composition, are considered: direct laser ablation of a target of corresponding composition, laser ablation of a combined target composed of two different metals, laser irradiation of a mixture of two or more colloidal solutions, and laser ablation in reactive liquids. The properties of two-component bimetallic systems (Ag – Cu, Ag – Au), semiconductor nanocrystals (ZnO, CdSe), chalcopyrite nanoparticles, and doped oxide nanoparticles (ZnO : Ag, $Gd_2O_2 : Tb^{3+}$) formed as a result of single- and double-pulse laser ablation in different liquids (water, ethanol, acetone, solutions of polysaccharides) are discussed.**

Keywords: *laser ablation in liquid, nanoparticle synthesis, laser-induced processes.*

1. Introduction

In recent years, in view of the prospects of practical applications, increasing attention is paid to the development of methods for synthesising nanostructures and studying their physicochemical properties. Among the new methods for fabricating nanoparticles, the ones based on laser ablation in liquids [1 – 3] are of great interest. In contrast to chemically synthesised nanoparticles, the nanoparticles formed by laser ablation in liquids do not content foreign ions and surface-active materials, which is an undoubted advantage for a number of applications (for example, in medicine). Other advantages of laser ablation are universality (it can be used for metals, semiconductors, and insulators of different composition) and possibility of controlling the characteristics of synthesised particles by changing the irradiation parameters. In most cases laser ablation is used to produce particles of metals and their oxides, and there are relatively few works devoted to the synthesis of composite nanoparticles, in particular bimetallic particles of different structure (alloy or core – shell) and particles of complex composition. Nevertheless, composite systems are of undoubted interest, because their properties generally differ from those of similar single-component structures. For example, it was established that the catalytic ability of bimetallic nanoparticles exceeds that of monometallic particles [4]. In addition, the physical properties of composite particles can be varied by changing their component ratio. In this context, it is urgent to reveal the main physical factors determining the formation of nanocomposite particles under laser ablation of solids in liquids.

During laser ablation small clusters and particles are either directly emitted from the target surface or formed as a result of condensation in the decaying plume [5]. Generally, condensation leads to the formation of particles composed of several tens or more (up to several thousands) atoms/molecules. Particles begin to grow after a decrease in temperature during adiabatic expansion of the plasma plume to supersaturation. Large particles are mainly the result of detachment of the target material due to different hydrodynamic mechanisms.

Particles of complex composition are formed during laser ablation due to the chemical reactions of target atoms with each other and with the environmental molecules [3]. The possibility of synthesising new (in particular, metastable) materials, which cannot be obtained under equilibrium conditions, is an important advantage of pulsed laser ablation in liquids (PLAL). This possibility was confirmed, in particular, by the experiments on fabricating cubic boron nitride and diamond nanoparticles [3, 6] and oxide semiconductor nanocrystals [7, 8] using the corresponding chemical reactions at high temperature and pressure, which occur in the initial stage of laser plume formation [9].

The concentrations of components in the laser plume and its temperature directly affect the processes leading to particle synthesis. Therefore, it is important to know the dynamics of plume composition evolution to optimise the PLAL conditions for fabricating nanoparticles.

In this review we generalize the results of the studies devoted to the formation of composite nanoparticles of controlled composition, structure, and size under laser ablation of solid targets in liquid media. Several approaches for implementing laser ablation in liquids to synthesise nanoparticles of complex composition are described. The properties of nanoscale bimetallic particles (Ag – Cu, Ag – Au), semiconductor nanocrystals (ZnO, CdSe), and some other nanoparticles formed by single- and double-pulse laser ablation in different liquids are considered.

N.V. Tarasenko, A.V. Butsen B.I. Stepanov Institute of Physics, National Academy of Sciences of Belarus, prosp. Nezavisimosti 68, 220072 Minsk, Belarus; e-mail: tarasenk@imaph.bas-net.by

Received 19 August 2010; revision received 23 September 2010
Kvantovaya Elektronika **40** (11) 986 – 1003 (2010)
Translated by Yu.P. Sin'kov

2. Characteristics of laser-ablation plasma in a liquid

The interaction of high-intensity pulsed laser radiation with a solid target in a liquid leads to the formation of a dense plasma cloud with rapidly changing parameters above the target surface. The plasma formed is expanded with a supersonic speed, being cooled as a result of electron–ion radiative recombination and chemical reactions. The radiative stage of laser-induced plasma is rather short (generally several hundreds of nanoseconds) [10–13]. A hemispherical cavitation bubble, composed of gaseous ablation products and vapour of the surrounding liquid, is formed after the plasma decay [14–16]. Having been formed after the laser pulse, the gas bubble continuously expands, reaches a maximum size for several hundreds of microseconds (depending on the target material and laser pulse energy), and then collapses [14, 15].

The parameters of laser-induced plasma determine the character of nanoparticle nucleation and growth. The atoms and clusters rapidly combine into small nuclei of nanoparticles and then grow by capturing clusters and free atoms. Therefore, the composition of the laser plasma formed during ablation (in particular, the atomic density in the gas phase) and the plasma temperature play an important role in the nanoparticle growth. One of the ways to control the sizes of the formed nanoparticles is to change the component composition of the laser plasma, which can be done, in particular, by varying the laser laser fluence on the target.

The laser-induced effects, which arise upon interaction of radiation with the target surface and near-surface plasma, can be used to control the laser plume characteristics. In this context, the technique of double-pulse laser ablation is of interest [11, 15, 17, 18]. Here, two successive laser pulses are used (Fig. 1): the first forms a gas cavity (gas bubble) from the ablation products, while the other induces a plasma plume. Currently, double-pulse laser ablation is successfully used in the laser-induced breakdown spectroscopy (LIBS), because this technique allows one to significantly increase the sensitivity for a number of elements in various objects, including those immersed in aqueous media [15, 19–22]. The advantages of the double-pulse laser ablation in liquids for nanoparticle synthesis were discussed in [23, 24], where, in particular, it was shown that, with the same number of irradiating laser pulses, the particle production rate in the double-pulse regime exceeds that in the single-pulse regime. Previously such synergism was also observed in the fabrication of carbon nanotubes using double-pulse laser ablation in a gaseous medium [25, 26].

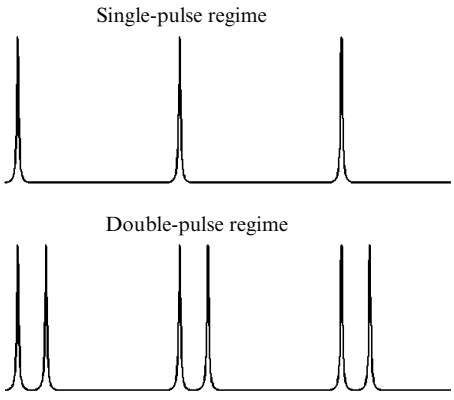

Figure 1. Sequence of laser pulses in the single- and double-pulse ablation regimes.

Experiments on obtaining nanoparticles and spectroscopic diagnostics of laser plasma in liquids were performed on the setup schematically shown in Fig. 2. The radiation sources were two Nd:YAG lasers (LOTIS LS21) with a pulse duration of 10 ns and a pulse repetition rate of 10 Hz, operating at the first (1064 nm) and second (532 nm) harmonics. The laser radiation was focused on the surfaces of metal targets (Ag, Au, Cu) or a combined target, composed of closely pressed plates of two metals. The target was placed in a cell with a liquid (ethanol, acetone, distilled water). The power density on the target surface could be varied from 10^8 to 5×10^9 W cm^{-2}.

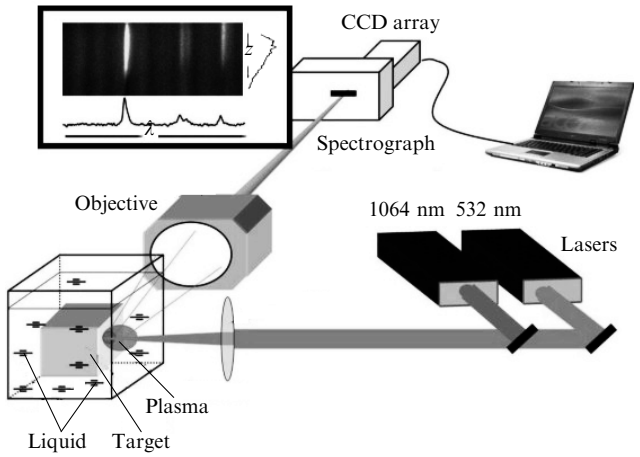

Figure 2. Experimental setup for time- and space-resolved spectroscopy of laser plasma.

Two regimes of laser ablation were applied: the single-pulse regime, where plasma was formed by irradiating a target with a 532-nm laser pulse, and the double-pulse regime, where the second 532-nm laser pulse followed with some delay ($\tau \leqslant 100$ μs) the first 1064-nm pulse. The laser beams were aligned on the target surface.

The experimental setup made it possible to analyse the time evolution of the plume emission spectra with a spatial resolution. The radiation was detected by a time-gated ICCD array (1024 × 256 pixels) with a minimum gate width of 10 ns. The typical gate steps were 100, 200, and 500 ns, and the gate widths were 50, 100, and 200 ns; they were chosen so as to obtain the optimal signal/background ratio and time resolution. The sensitivity of the CCD array with a brightness amplifier was approximately constant in the spectral range containing the chosen lines. The methods of plasma diagnostics were described in detail in [27].

The data on the laser plume size and shape were obtained using the technique of time-resolved image detection [27]. Typical images and intensity distributions for the luminous region of the plasma plume are shown in Fig. 3. An analysis of the images obtained shows a significant difference in the character of plume formation and evolution in liquid and in air. One can see from Fig. 3 that the size and lifetime of plasma in a liquid are several times smaller than

for the plasma in air in both single- and double-pulse ablation regimes. The main differences between the laser ablation in a liquid and in a gas (vacuum) are due to the fact that in the former case the plasma plume expansion is hindered by the surrounding liquid, and this circumstance significantly affects the thermodynamic and kinetic aspects of plume evolution and condensation in the plume. In particular, the shock wave generated by the expanding plasma plume in the presence of a liquid increases the temperature and pressure of the initial laser-induced plasma [28]. The high-temperature and high-density state of the plasma is favourable for endothermic chemical reactions, and the short lifetimes of these states facilitate the formation of metastable phases of the structures synthesised [3].

When decaying in a liquid (in both gas and vacuum), laser plasma is cooled and ablation products are condensed. Most condensation products are dispersed in the liquid to form nanoparticles, whose parameters are eventually determined by the thermodynamic state of decaying plasma (its temperature and atomic and ionic densities). The more rapid

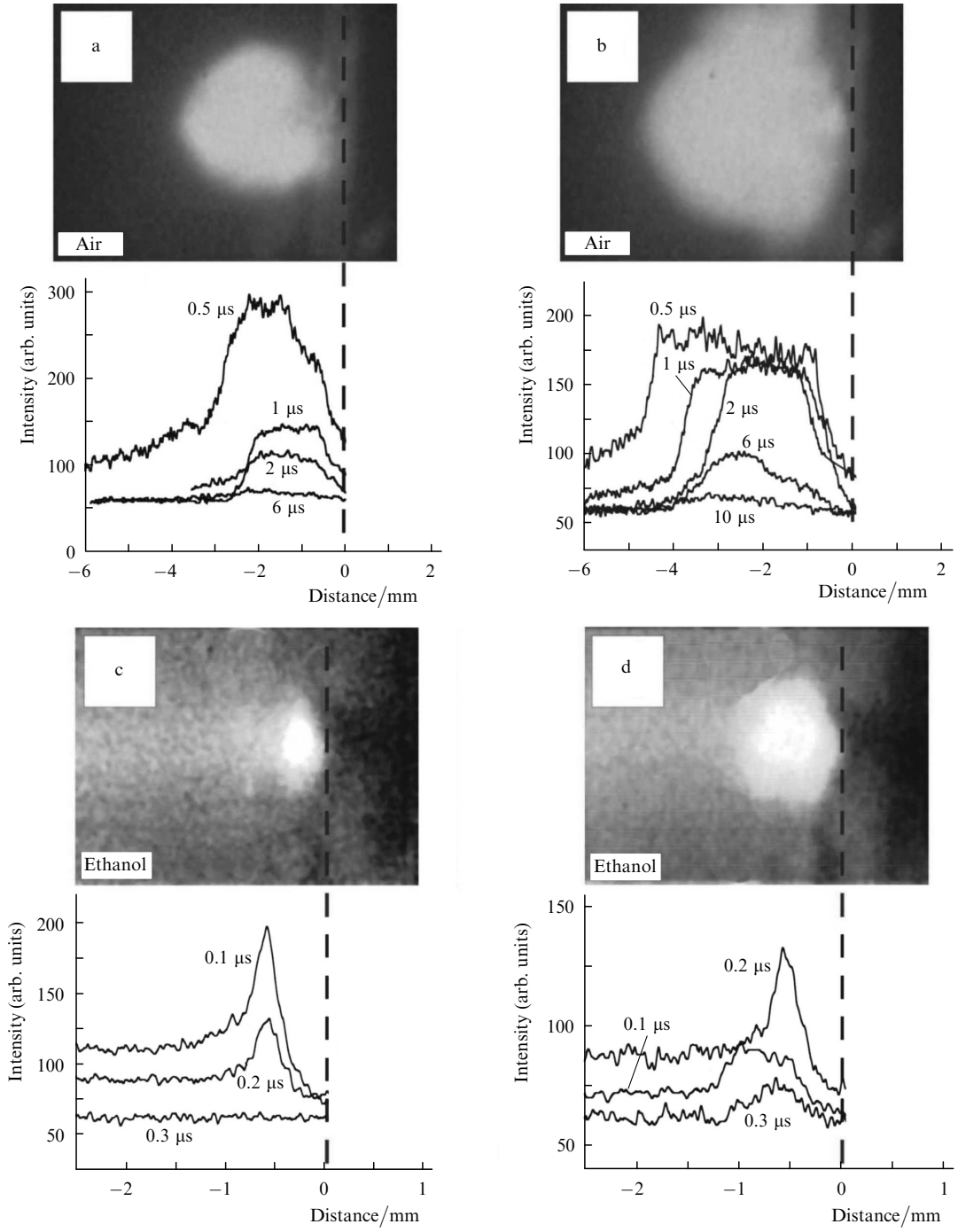

Figure 3. Plasma plume images recorded (a, b) 1.5 μs and (c, d) 200 ns after laser irradiation and the corresponding radiation intensity distributions (at different instants) for the plasma formed in the (a, c) single-pulse and (b, d) double-pulse (1064 and 532 nm) regimes of ablation of a copper plate in air and ethanol, recorded along the normal to the target surface. The position of the target surface is shown by the dashed lines. The time windows for image detection are 100 and 50 ns for the plasma plumes in ethanol and air, respectively.

decay of the laser-induced plasma in the liquid limits the growth of the formed particles [29].

The atomic (ionic) density in the laser-induced plasma in the liquid can be estimated by measuring the plasma volume (the size of the image of luminous region in the plume) and calculating the amount of the ablated target material. The mass of the ejected material, determined by weighing a copper target before and after the irradiation by laser pulses of specified width and repetition, turned out to be 4.7×10^{-5} mg pulse^{-1}. On the assumption that the mass of the ejected target material depends linearly on the number of laser pulses and that the evaporated material is completely atomised, the concentration of copper atoms in the plasma was 1.4×10^{19} cm^{-3}.

The temperature of laser plasma and concentration of charged particles in it can be determined by analysing the plasma emission spectrum. Fragments of time-integrated spectrum of the laser plume (500 – 525 nm), recorded during single- and double-pulse ablation of a copper target in water, with different time delays between the laser pulses, are shown in Fig. 4. One can see that continuous radiation dominates in the plasma spectrum in the case of single-pulse ablation. The continuous emission spectrum is determined by such processes as electron – ion radiative recombination and bremsstrahlung. It should be noted that, as the time-resolved measurements showed, the emission signal disappeared after several hundreds of nanoseconds due to the rapid cooling of plasma [30]. An intense continuous spectrum dominates also in the case of double-pulse ablation at short delays of the detection gate. An increase in the delay time in the case of double-pulse ablation leads to the manifestation of individual spectral lines of target atoms.

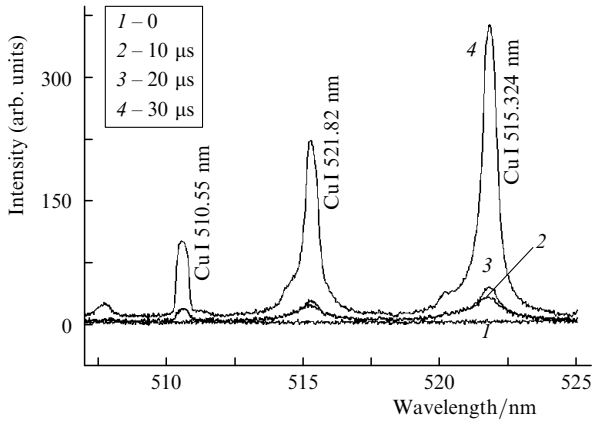

Figure 4. Fragments of the time-integrated spectrum of the laser plasma, obtained under (*1*) single-pulse and (*2–4*) double-pulse (with different time delays between the pulses) ablation of a copper target in water.

The fact that the copper emission lines are more pronounced for double-pulse irradiation in comparison with the single-pulse regime is explained as follows. The second pulse induces plasma in the gas bubble that is formed as a result of the decay of the first-pulse plasma. After the first pulse the plasma expands and recombines, and its electron density decreases with time. The second pulse passes through a relatively rarefied medium and, therefore, efficiently interacts with the surface. As a result, the signal increases, both due to the increase in the amount of the evaporated target material and because of a more uniform distribution of density and temperature in the resulting plasma. The spectra in Fig. 4 reflect the time evolution of the pressure and temperature in the gas bubble during its expansion.

The radiation spectrum of laser plasma in the liquid was used to estimate the temperature and electron concentration. The electron temperature of the plasma was determined (on the assumption that the conditions of local thermodynamic equilibrium are satisfied and the self-absorption processes are negligible for the copper transitions) from the Boltzmann distribution of populations over the Cu I lines at 510.55, 515.324, and 521.82 nm. The electron temperature of the plasma in the double-pulse regime was found to range from 0.8 eV (at the plume periphery) to 1.4 eV (in the central part of the plume).

The electron density of the laser plasma in the liquid was determined by analysing the profiles of the 515.324- and 521.82-nm Cu I lines, which are broadened as a result of the quadratic Stark effect. Under our experimental conditions, the effect of interactions of other types on the spectral line broadening was much smaller and could be assigned to the error in measuring the linewidth. The electron concentration was found (from the experimental linewidths) to vary from 2×10^{18} cm^{-3} in the central part of the plume to 1×10^{18} cm^{-3} at its periphery.

3. Properties of the nanoparticles formed under single- and double-pulse laser ablation in a liquid

Generally, nanoparticle formation during laser ablation in liquids is primarily monitored by recording the absorption spectra of colloidal solutions. The absorption spectra of colloidal solutions of silver, gold, and copper have characteristic absorption bands peaking at about 400, 520, and 570 nm for silver, gold, and copper nanoparticles, respectively. These bands are known to be due to the collective excitation of conduction electrons of the metal (the so-called surface plasmon resonances) [31]. The presence of a single absorption band in the spectrum indicates that the particle shape is close to spherical. The absorption spectrum of ellipsoidal particles contains two absorption peaks [32].

Taking into account the wavelength dependence of the optical constants of spherical particles with respect to the environment, their absorption spectra are described within the Mie theory [31]. The position, width, and amplitude of resonances depend on the dielectric constants of the metal and environment, the particle morphology, and the presence (absence) of adsorbents on the particle surface [33]. Non-interacting spherical particles exhibit a single resonance until the inequality $r \ll \lambda$ is valid, where r is the particle size and λ is the incident light wavelength. The metal particles formed by laser ablation have typical sizes of 3 – 20 nm. In this range there is no strong dependence of the absorption spectra on the particle size; however, with a change in the size distribution of the formed particles and the degree of their aggregation the maximum in the spectrum may shift. Note that the absorption spectra of colloidal metal particles have been intensively experimentally studied; in particular, the effect of changes in the particle size and on the spectra was analysed in [32, 34]. Nevertheless, the formation of the spectra is far from being clearly understood. The experimental spectra are significantly affected by

polydispersity, presence of aggregates, and deviation of particle shape from spherical.

Note that the copper nanoparticles formed in water are not stable: a half an hour after the laser irradiation a precipitate arises in the cell, and the band due to the plasmon absorption (peaking at about 580 nm) disappears. Copper particles are more likely to be oxidised by the oxygen atoms dissolved in water [35]. At the same time, using ethyl alcohol as a working liquid, one can obtain more stable nanoparticles. A series of experiments on laser ablation of a copper plate in acetone showed that the stability of copper nanoparticles obtained in this liquid exceeds that of the particles obtained in ethanol. The ability of acetone to stabilise metal silver nanoparticles was described in [36, 37]. The stabilising effect of acetone can be explained in terms of the interaction of the carbonyl group of acetone molecules with the particle surface, which leads to the formation of a protective dipole layer, hindering the particle aggregation.

In our experiments the intensity and shape of the absorption bands of nanoparticle solutions depended also on the ablation regime. As was shown in [23], the double-pulse ablation in liquids is more efficient than the single-pulse one.

The use of double-pulse laser ablation, either a combination of two 1064-nm pulses or a 1064-nm pulse followed by a 532-nm pulse, led to changes in the absorption spectrum of the formed particles (Fig. 5). The colloids formed by double-pulse ablation, exhibit a higher optical density (with the same total number of laser pulses) in comparison with the single-pulse ablation. In addition, the absorption spectrum becomes more symmetric and less red-broadened.

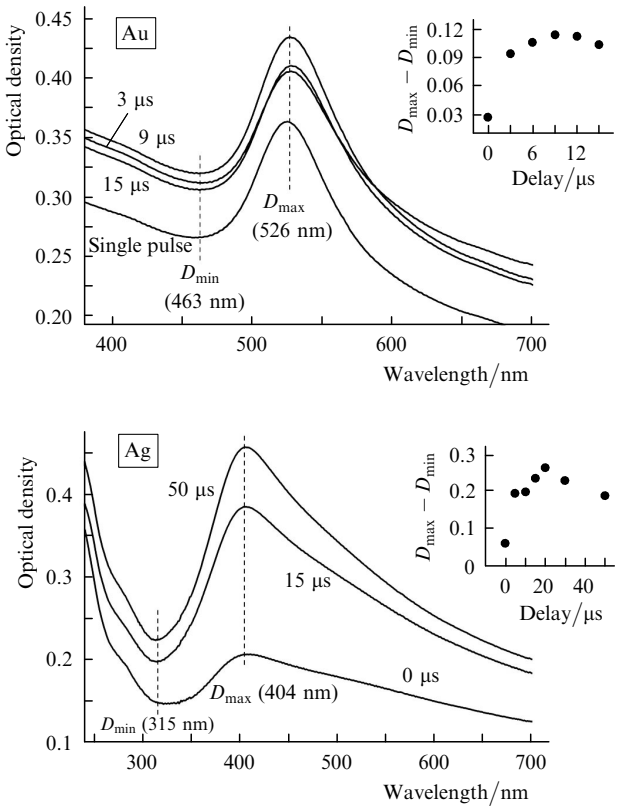

Figure 5. Absorption spectra of the solutions of gold and silver nanoparticles formed during double-pulse laser ablation in ethanol at different delays between the pulses. The insets show the dependences of the differences in optical densities $D_{max} - D_{min}$ on the delay time.

The spectral features observed depend on the time delay between the laser pulses (Fig. 5, inset). The optimal time delays are within 10–20 μs and 10–12 μs for silver and gold nanoparticles, respectively. The aforementioned changes in the absorption spectra indicate the difference in the size distribution functions of the particles (smaller sizes of the particles formed by double-pulse ablation). The micrographs confirmed that the particles formed by double-pulse ablation were smaller than those produced in the single-pulse regime by a factor of 2–3 [23]. The particles are most likely to decrease in size as a result of their heating and fragmentation by the second laser pulse (if appropriate time delays are chosen).

4. Laser synthesis of bimetallic nanoparticles

According to the data in the literature, different laser-induced processes were used to fabricate bimetallic nanoparticles. For example, laser ablation of metal alloy targets in a liquid was used to produce gold–silver alloy [38] and brass [39] particles. Nanoparticles of a metastable silver–nickel alloy were synthesised using a cw CO_2 laser and pulsed Nd:YAG laser in nitrate and acetate precursors of silver and nickel [40] and Au–Ag alloy nanoparticles were fabricated by a two-step technique: laser ablation of pure metal samples in water and subsequent irradiation of the mixture of colloidal solutions [41]. Formation of alloy nanoparticles as a result of laser irradiation of Au–Ag nanoparticles with a core–shell structure was reported in [42, 43]; it was believed in these studies that the interaction of laser radiation with nanoparticles changes the particle composition through alloying. In some cases an analysis of the absorption spectra made it possible to establish unambiguously whether bimetallic Au–Ag nanoparticle had a core–shell structure or were alloyed.

Pulsed laser ablation in liquids was used to obtain composite particles with metal–metal, semiconductor–metal, metal–semiconductor, and semiconductor–semiconductor structures [41, 44, 45], including nanoparticles with a metal core and oxide shell, for example, Zn–ZnO and Sn–SnO_2 [45, 46]. It was recently reported [47] about the use of laser ablation of a metal target (Sn) in a solution of particles of another metal (Au) to form shell Au–SnO_2 nanoparticles. The formation of a thin shell around a nanoparticle was considered to occur as a result of deposition of the ablation products of the other metal.

A similar approach, based on successive laser ablation of different targets in the same solution, can also be used to obtain mixtures of different particles. In this case, the relative concentration of nanoparticles of different materials can be controlled by varying the processing time of each target.

In our experiments bimetallic Ag–Cu and Ag–Au nanoparticles were synthesised by laser ablation of a combined target (Fig. 6), composed of two plates of the corresponding metals, for example, silver–copper or silver–gold [24]. The target was placed in a cell with a liquid (acetone or ethanol), and ablation was performed by the second harmonic of yttrium aluminium laser (532 nm). The laser beam was focused at the interface between the two metals into a spot 0.5 mm in diameter; the laser fluence on

the target surface was 15 J cm^{-2}. Colouring of the liquid was observed during ablation, which indicated the formation of nanoparticles from the target material. Based on the detected changes in the absorption spectra of colloidal particles of individual metals and their composites and the electron microscopy and X-ray diffraction data, the composition and structure of the particles formed were established.

Transmission electron microscopy (TEM) images of single-metal silver and copper particles and the particles formed by laser ablation of a two-metal (Ag – Cu) joint are shown in Fig. 7. One can see that the average size of silver particles is about 15 nm and that the size distribution is asymmetric within 5 – 50 nm. The average size of copper particles formed under the same experimental conditions is 10 ± 2 nm. According to the data in Fig. 7, ablation of a combined Ag – Cu target leads to the formation of particles with an average diameter of 5 – 7 nm. Note that the size distribution of these particles is not bimodal, which indicates that the colloidal solutions obtained in this case are not mixtures of particles.

The optical spectra of the three samples fabricated by laser ablation in ethanol (colloidal solutions of single-metal silver and copper particles and a solution prepared by ablation of a combined Ag – Cu target) are shown in Fig. 8. All spectra demonstrate characteristic absorption bands with maxima; they are due to the collective excitation of conduction electrons. Silver particles exhibit maximum absorption near 405 nm, while the solution of copper particles is characterised by absorption in the entire visible range, with a small peak near about 570 nm. Note that the experimental absorption spectra of colloids of individual

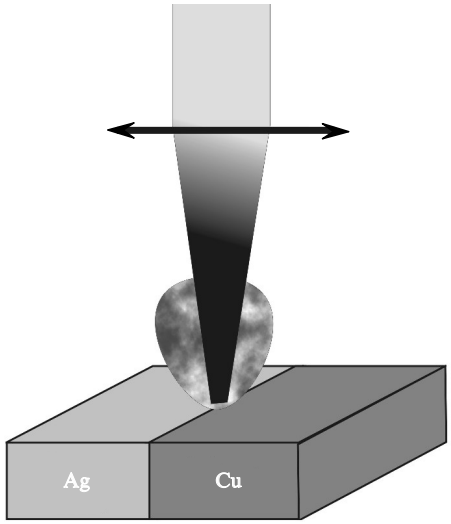

Figure 6. Schematic diagram of the effect of a laser beam on a combined target.

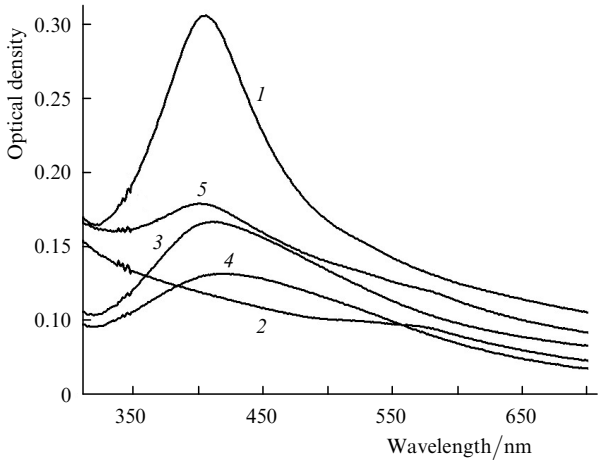

Figure 8. Optical absorption spectra of (*1* – *4*) the colloidal nanoparticle solutions obtained in ethanol under laser ablation ($\lambda = 532$ nm) of (*1*) silver, (*2*) copper, and (*3*, *4*) combined Ag – Cu target at different concentration ratios of elements in the laser plume and (*5*) a mixture (with a volume ratio of 1 : 1.4) of silver and copper colloids in ethanol.

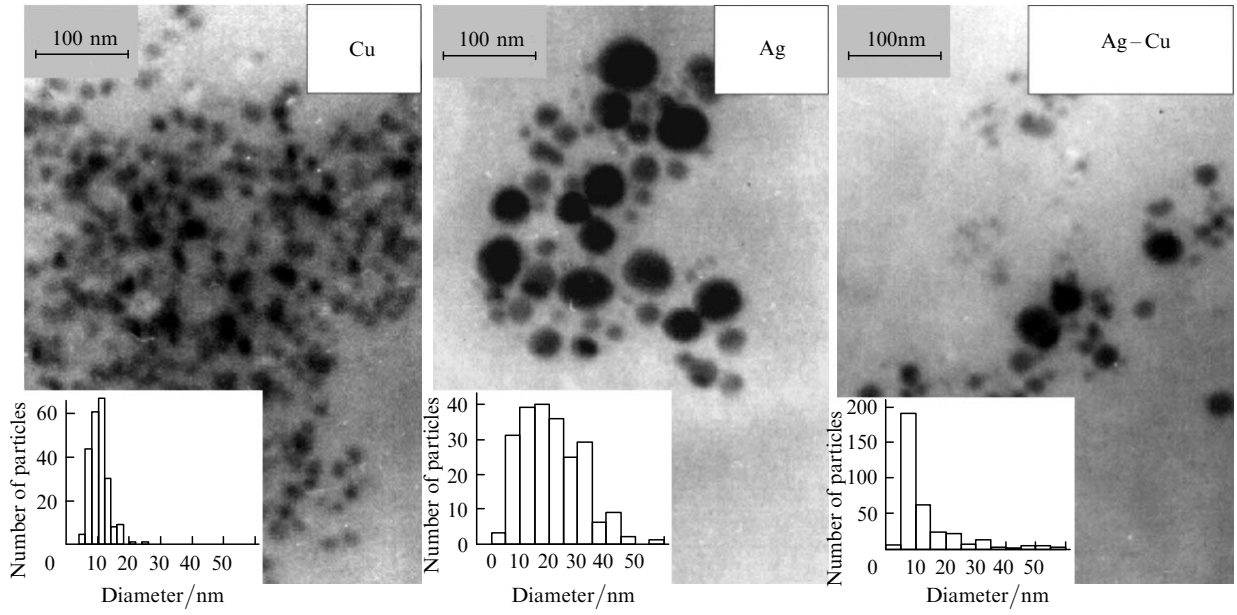

Figure 7. TEM images of copper and silver nanoparticles and bimetallic Ag – Cu particles obtained by laser ablation of the corresponding targets in ethanol for 3 min and the histograms of particle size distributions.

metals are in good agreement with the data in the literature [33].

The absorption spectrum of the solution obtained by ablation of a combined Ag–Cu target differs from both the spectra of single-metal silver and copper particles and the spectrum of a mixture of these particles. A single absorption band, with a maximum red-shifted with respect to the absorption maximum of silver particles, is observed in the case of ablation of the combined Ag–Cu target. In addition, the absorption peak of copper particles is absent, and the band is somewhat red-broadened. The spectral shape depends on the concentration ratio of elements in the laser plume, which was varied by changing the ratio of the irradiation spot areas for both metals in the focal region of the lens focusing the laser radiation on the target. In this case, it is rather difficult to quantitatively determine the proportion between the silver and copper atoms formed; nevertheless, one can reveal the general tendency in the change in the spectral shape.

With an increase in the amount of copper in the ablation plume, which was implemented by displacing the focal spot toward the copper target, the absorption peak broadened and shifted to the red region [Fig. 8, curve (*4*)]. In this case, no significant increase in the absorption in the range of plasmon resonance of copper nanoparticles was observed. The frequency of the surface plasmons of silver nanoparticles and the interband transition frequencies are known to lie in different wavelength ranges; whereas the plasmon absorption of copper nanoparticles is imposed on the interband absorption. Therefore, the red shift is likely to be caused by the change in the dielectric function of the particles, which is due to the formation of two-component nanoparticles [34, 48].

Note also that the absorption curve for the solution of Ag–Cu particles cannot be obtained by simple addition of the absorption curves of silver and copper solutions. The spectrum of a mixture of silver and copper particles, obtained by combining the two corresponding solutions, has two absorption peaks due to single-metal particles [curve (*5*)]. The absence of two plasmon peaks in the spectrum of colloids formed as a result of laser ablation of a combined target indicates that these colloids are not mixtures of individual-metal particles but consist of particles with a mixed composition. One would expect two plasmon bands for a mixture of individual particles with a band intensity ratio dependent on the component ratio in solutions [43, 49].

The above-described method was also approved for laser ablation of a joint between silver and gold plates in ethyl alcohol. The TEM images of the particles formed are shown in Fig. 9a. Two pronounced bands, peaking at 405 and 540 nm, were observed for the solutions prepared by separate ablation of these targets [Fig. 9b; curves (*1*, *2*)]. Absorption bands with single maxima at about 430 and 445 nm were observed in the case of ablation of a two-sample joint [curves (*3*, *4*)]. These peaks are located between the maxima of the plasmon bands of single-metal silver and gold particles; therefore, the spectra recorded correspond to the plasmon absorption of alloy particles. The plasmon absorption maxima of bimetallic Ag–Au particles shift away (linearly) from the maximum of single-metal silver particles, proportionally to the increase in the gold content in the particles [38]. These spectral features indicate that the Ag–Au particles formed by the above-described method are homogeneously alloyed nanoparticles.

The elemental composition of the bimetallic particles formed was determined using energy-dispersive X-ray (EDX) analysis; a typical result for Ag–Cu particles is shown in Fig. 10. The EDX spectra indicate the presence of both metals in the particles under study; no other elements were detected.

The phase composition of the synthesised particles was determined by X-ray diffraction (XRD) analysis. Diffraction peaks were identified and the lattice parameters of silver and bimetallic particles were determined. The diffraction pattern of the powder of particles obtained by laser ablation

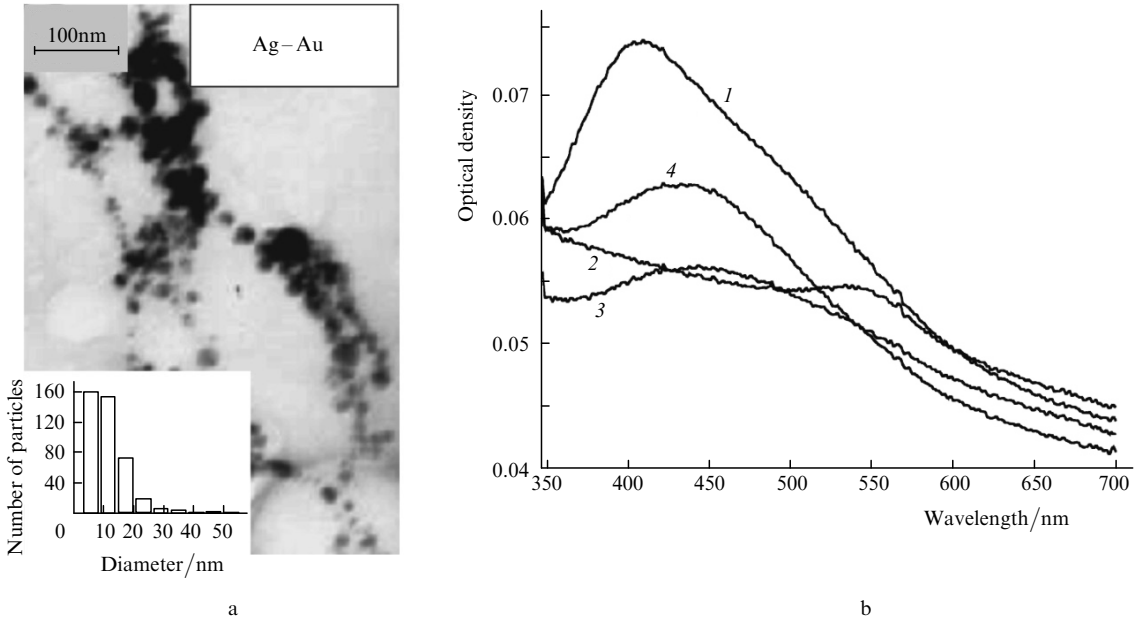

Figure 9. (a) TEM images and (b) the optical absorption spectra of colloidal nanoparticle solutions obtained under laser ablation ($\lambda = 532$ nm) of a (*1*) silver, (*2*) gold, and (*3*, *4*) combined Ag–Au target in ethanol, at different concentration ratios of elements in the laser plume.

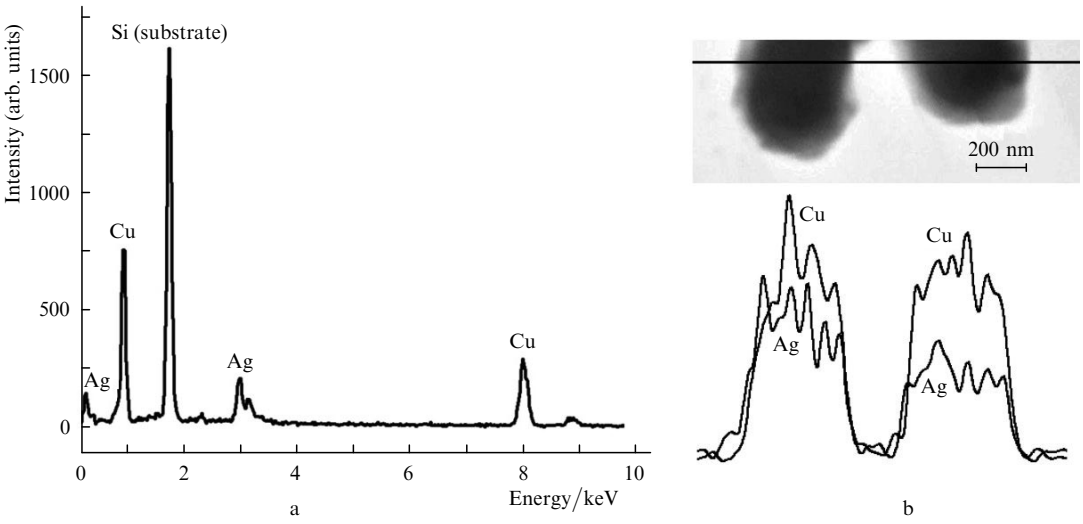

Figure 10. (a) Elemental composition and (b) distribution of elements along the observation line for a powder synthesised by laser ablation of a combined Ag–Cu target.

of an Ag–Cu joint contains reflections of both silver and copper of cubic structure, with the lattice constants $a = 4.08610$ and 3.61505 Å, respectively. This finding, as was suggested above, agrees with the formation of bimetallic particles composed of crystalline silver and copper clusters. In the case of formation of alloyed nanoparticles the diffraction pattern should contain alloy reflections. The presence of a single band in the optical absorption spectrum, with a position dependent on the concentration of a particular metal, may indicate the alloy formation. However, since silver and copper are characterised by low mutual solubility, particles composed of nuclei of silver and copper crystalline phases are more likely to be formed [49].

Bimetallic Au–Ag nanopowders had the same XRD structure as pure Ag and Au particles: four diffraction peaks at $2\theta = 38.2^\circ$, 44.3°, 64.5°, and 77.6° from the (111), (200), (220), and (311) planes, respectively. Because gold and silver have the same structure (fcc) and very close lattice constants (0.408 and 0.409 nm, respectively), their XRD reflections are practically identical, and, therefore, one cannot distinguish a gold–silver alloy from a single-metal (Au or Ag) phase based on only the XRD data.

As ideal solid solutions are formed at any concentration ratio of Ag and Au, alloying of these two metals is thermodynamically favourable, and the material of the nanoparticles formed is a homogeneous alloy.

Thus, laser ablation of a combined target in the liquid yields Ag–Cu and Ag–Au nanocomposite particles. The absorption spectra of the nanoparticles exhibit a plasmon resonance, which lies between the resonances of the corresponding single-metal particles. The peak position changes with a change in the size ratio for the combined-target irradiation spots; this correlation is indicative of a change in the element concentration ratios in particles. The optical absorption spectra showed that the particles synthesised by laser ablation of combined samples are not a mixture single-metal nanoparticles, but each particle has a mixed composition. As follows from the TEM data, the sizes of single-metal and bimetallic particles differ (bimetallic particles are smaller than silver ones). The technique developed is expected to be useful to produce other two-component systems.

5. Formation of nanoparticles under laser ablation of complex-composition targets in liquids

Pulsed laser ablation in liquids makes it possible to obtain nanostructures of different composition using combinations of different solid targets and liquids. In particular, we used PLAL to form nanoparticles of chalcopyrite ($CuFeS_2$) and cadmium selenide (CdSe) under laser ablation of corresponding targets and gadolinium carbide nanoparticles under ablation of metallic gadolinium target in carbon-containing media (ethanol and acetone) [17, 50].

Chalcopyrite nanoparticles were synthesised by laser sputtering of a sample of the original mineral in water. The phase and elemental compositions of the particles formed were analysed by XRD and EDX.

A chalcopyrite target was placed in a cell with distilled water and irradiated by a Nd:YAG laser ($\lambda = 1064$ nm, energy per pulse 60 mJ, pulse repetition rate 10 Hz, and pulse duration 12 ns). The small plasma plume was formed during ablation above the target surface. While particles were formed, the liquid became visibly coloured. The particles synthesised formed a colloidal solution.

The optical absorption spectra of as-prepared colloidal chalcopyrite solutions are gradually decaying curves, which show a tendency to a gradual decrease in the total absorption with an increase in the wavelength. The relative contents of Fe, Cu, and S atomic components in the formed particles, determined from the EDX spectrum, corresponded to the stoichiometric ratio for the $CuFeS_2$ phase. Although the EDX analysis allowed the presence of oxides, the XRD analysis did not reveal any oxide phases in the sample. This fact suggests that the samples under study contained oxygen-absorbing impurities (for example, carbon atoms, which are always present on the sample surface).

As can be seen in the diffraction pattern (Fig. 11), the synthesised powder consists of tetragonal chalcopyrite $CuFeS_2$ (diffraction peaks at $2\theta = 29.5^\circ$, 48.7°, 49.1°, 57.9° and 58.7°). Note that there are few small peaks from the $CuFe_2S_3$ and $Cu_2Fe_4S_7$ phases near the diffraction peaks of $CuFeS_2$. Thus, the formation of metastable copper-

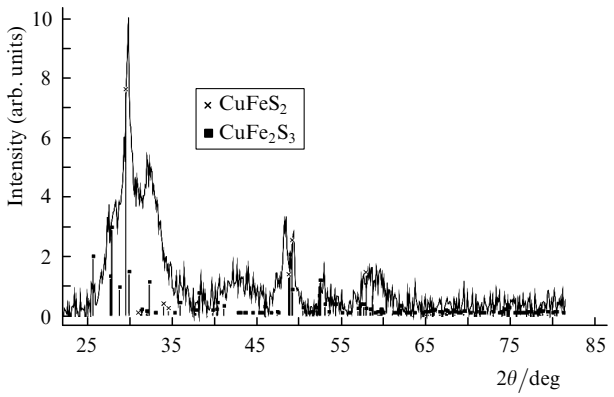

Figure 11. Diffraction pattern of the nanoparticles obtained by laser ablation of a chalcopyrite target.

and iron-containing compounds is not excluded. However, oxide phases were not observed.

The study of the synthesised particles by IR Fourier spectroscopy revealed bands between 1094 and 1200 cm^{-1}, which can be considered as characteristic bands of chalcopyrite [51, 52]. The peak positions for the synthesised powders somewhat differ from those for the bulk material, which can be caused by the formation of metastable phases.

The atomic force micrographs of the chalcopyrite particles deposited on a mica substrate showed agglomerates of nanoparticles, which were most likely formed during deposition. The initial particles were of approximately the same size (50 – 100 nm).

It is noteworthy that the formation of stoichiometric nanoparticles under laser ablation of chalcopyrite in water is rather unexpected. Conservation of stoichiometry during pulsed laser ablation of combined semiconductors in liquids was previously reported in [53]. The formation of CdS and ZnSe semiconductor nanocrystals was observed during laser ablation of the corresponding single crystals in some liquids (diethylene glycol, isobutanol, ethanol, dimethyl sulfoxide). It was suggested in [53] that CdS and ZnSe remain stoichiometric due to the high vapour density of the surrounding liquid, which impedes dissociation of molten semiconductor nanoparticles into components.

In summary we should note that, according to our experimental data, laser ablation of cadmium selenide single crystals in ethanol by the second harmonic of Nd : YAG laser also leads to the formation of particles with the corresponding stoichiometry. The typical shape of the CdSe nanoparticles obtained by laser ablation is shown in Fig. 12. One can see that spherical particles with an average diameter of 25 nm are formed at an laser fluence of 0.2 J cm^{-2}.

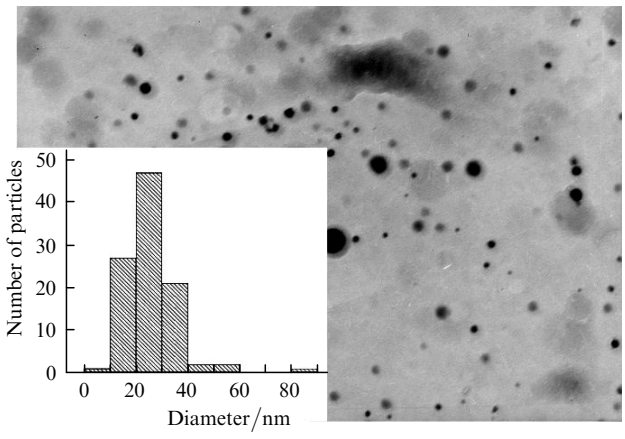

Figure 12. CdSe nanoparticles formed by laser ablation (Nd : YAG, second harmonic) of CdSe in ethanol.

6. Laser synthesis of zinc oxide nanostructures

Oxide particles can be obtained either by direct laser ablation of a solid oxide target or using ablation of the corresponding metals in reactive liquids. Synthesis of nanocrystals of different oxides, including TiO_2, SnO_2, etc., was reported in a number of studies [29, 46, 54, 55]. In particular, very small (3 – 5 nm in diameter) TiO_2 nanoparticles were formed by pulsed laser ablation (third harmonic of a Nd:YAG laser, pulse repetition rate 10 Hz, pulse duration 7 ns) of a titanium target immersed in an aqueous solution of sodium dodecyl sulfate [$C_{12}H_{25}SO_4Na$ (SDS)] and in deionised water [29]. The use of SDS solution prevents aggregation of the obtained particles; the size of noble metal nanoparticles is controlled in the same way.

The possibility of applying pulsed laser ablation in the liquid to obtain ZnO nanocrystals was discussed in [8, 56 – 59]. For example, ZnO nanoparticles were formed by laser ablation of metallic zinc in deionised water [57], the mixture of water and isopropyl alcohol [59], deionised water mixed with hydrogen peroxide, and distilled water with simultaneous oxygen leaking and using sodium dodecyl sulfate as a surfactant to prevent nanoparticles from agglomeration [58]. In addition, ZnO nanocrystals with a narrow size distribution were formed in an acid or alkaline medium without adding a surfactant due to the increase in the surface charge of particles in comparison with the charge of those formed in deionised water. However, the ZnO nanoparticles formed in a NaCl solution rapidly agglomerated due to the decrease in the surface charge [57].

Zinc oxide is a wide-gap ($E_g = 3.37$ eV) semiconductor, which is promising for UV semiconductor lasers and LEDs. In comparison with other semiconductors, ZnO has a higher exciton excitation energy and is more radiation-resistant; in addition, it is a multifunctional material, which exhibits piezoelectric, ferroelectric, and ferromagnetic properties [60, 61]. Zinc oxide can be applied in solar cells, piezoelectric transducers, and as catalytic particles and sensors to determine the molecular gas composition. Finally, ZnO is an ecologically safe and biocompatible material, which is important for medical applications. To date, room-temperature ferromagnetism has been obtained in this material doped with vanadium, cobalt, and iron (generally, the fraction of magnetic ions is several percent). ZnO-based nanostructures are of particular interest because of their expected new properties related to surface and quantum-size effects.

Note that ZnO almost always exhibits n-type conductivity, and it is fairly difficult to obtain p-type samples [62]. To this end, it is necessary to find optimal dopants and ways for their incorporation into ZnO. Phosphorus, nitrogen, and other fifth-group elements are generally used as dopants. A dopant providing the necessary value and type of conductivity must not deteriorate the radiative characteristics and transparency of zinc oxide crystals.

In our experiments zinc oxide nanoparticles were synthesised by laser ablation of targets made of metallic zinc and pressed commercial ZnO powder, with their subsequent deposition on a silicon substrate. The composition, morphology, and optical properties of the formed structures were analysed. Ablation was performed by a Nd : YAG laser (wavelength, 1064 nm; energy per pulse, 50 mJ; repetition rate, 10 Hz). The target was fixed on the bottom of a glass vessel filled with distilled water. The laser beam was focused through a 2-cm water layer into a spot 0.4 mm in diameter on the target surface; the maximum laser fluence in the spot was about 250 J cm^{-2}.

The TEM images of the ZnO particles (Fig. 13) show details of their morphological structure. The micrographs exhibit weakly connected groups, composed of almost spherical particles. The average particle diameter ranges from 30 to 40 and from 15 to 20 nm for the laser ablation of a metallic zinc target and ZnO pellet, respectively.

The absorption spectra of the colloidal solutions of the nanoparticles are shown in Fig. 14. It can be seen that these solutions have broad absorption bands in the UV spectral range, with a rapid increase in absorption near the band gap edge, which is characteristic of semiconductors. The absorption spectra of the suspensions in the $(k \times hv)^2$, hv coordinates (k is the absorption coefficient and $E = hv$ is the photon energy) can be used to estimate the band gap. The absorption spectra of the particles obtained by laser ablation of Zn and ZnO targets give band gaps of approximately 3.10 and 3.18 eV, respectively (see Fig. 14b), i.e., values smaller than for the bulk material ($E_g = 3.37$ eV, according to [60, 63]). This can be caused both by the size effect and by the formation of defect levels near the bottom of the conduction band (for example, due to the ablation nonstoichiometry [64]).

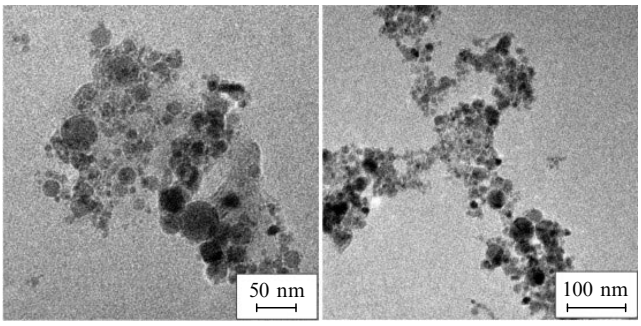

Figure 13. TEM images of the zinc oxide nanoparticles formed by laser ablation of metallic zinc (left) and pressed powder (right) targets in distilled water.

The X-ray diffraction patterns of the synthesised material contain clear reflections, which indicate the crystal structure of the samples. Peaks corresponding to hexagonal ZnO with the lattice parameters $a = 0.325$ nm and $c = 0.521$ nm were observed; they are in good correspondence with the JCPDS data for ZnO. The Scherrer formula $D_{cr} = 0.89\lambda_R/(\Delta \cos\theta)$ (D_{cr} is the crystallite size, λ_R is the X-ray wavelength, θ is the diffraction angle, and Δ is the reflection peak width at half maximum) was used to determine the crystallite size (~ 25 nm), averaged over peaks in the angular range under study. In the case of commercial zinc oxide powder, the average grain size was about 500 nm.

In the recent years, the photoluminescence properties of ZnO (which are important for determining structural defects and impurities in oxide structures) have been intensively studied. A UV luminescence band peaking near 380 nm and one or several bands in the visible range were observed for zinc oxide nanostructures excited at room temperature [65–68].

The luminescence spectra of the ZnO structures synthesised by laser ablation in water and deposited on a silicon substrate are shown in Fig. 15. The luminescence spectrum of a commercial ZnO powder is also presented for comparison. The luminescence spectrum of the ZnO sample synthesised by laser ablation of a ZnO target exhibits a strong UV luminescence band peaking at about 380 nm and relatively weak violet luminescence. The green band, which correlates with oxygen vacancies, is absent. For the samples obtained by laser ablation of metallic zinc, the luminescence spectrum has two peaks: at 416 and 435 nm. The spectrum of the sample prepared from a commercial ZnO powder contains a relatively weak UV band (383 nm) and a wide green band peaking at about 515 nm.

Several mechanisms were proposed to explain the photoluminescence properties of ZnO nanostructures. The UV luminescence band at about 380 nm is assigned to the recombination emission of electron–hole pairs [65]. The occurrence of bands in the visible range is due to different point structural defects (induced by doping) or internal lattice defects. In particular, the violet luminescence of the

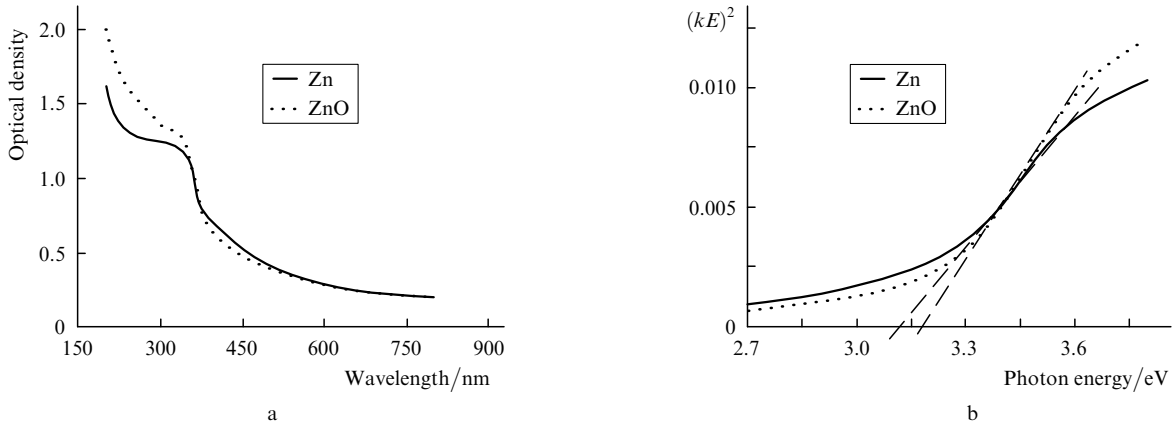

Figure 14. (a) Absorption spectra of colloidal zinc oxide solutions synthesised by laser ablation of metallic zinc and pressed ZnO powder in distilled water and (b) the dependence of $(kE)^2$ on the photon energy hv.

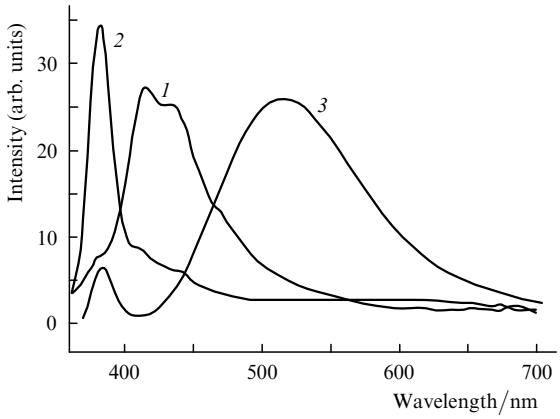

Figure 15. (*1*, *2*) Luminescence spectra of the zinc oxide structures (excitation wavelength 270 nm) obtained by laser ablation of (*1*) Zn and (*2*) ZnO targets in water and (*3*) the spectrum of commercial zinc oxide powder.

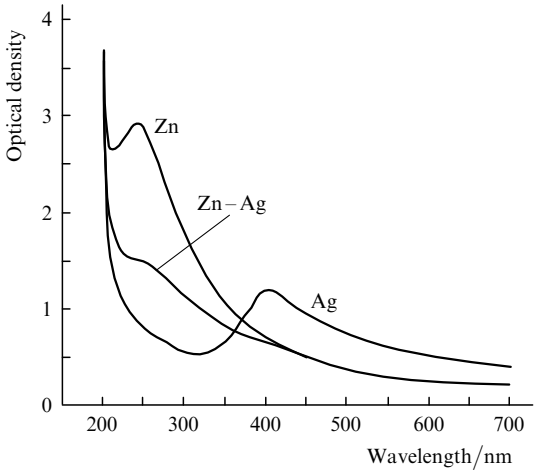

Figure 16. Optical absorption spectra of the colloidal solutions obtained by laser ablation of zinc, silver, and combined Zn – Ag target in distilled water.

sample prepared by laser ablation of a zinc target [Fig. 15, curve (*1*)], can be caused by the presence of defects of zinc interstitial and oxygen vacancy types.

The most often observed green band with a maximum in the range of 450 – 550 nm is assigned to oxygen vacancies. Annealing of powders in oxygen atmosphere generally leads to a decrease in the intensity of this band and increase in the UV maximum [69]. In addition to this generally accepted hypothesis, the presence of hydroxide particles on the surface was interpreted as a possible cause of weak UV and stronger yellow-green luminescence [68]. The orange-red luminescence with a maximum in the range of 640 – 650 nm is generally related to the presence of surface dislocations or defects of interstitial zinc type [68].

Note that, according to our measurements, the ZnO nanostructures deposited on the substrate exhibited stronger UV luminescence in comparison with the ZnO nanoparticles in colloidal solutions, whose spectrum contained a strong orange-red band. The ratio of the UV- and visible-band intensities in the ZnO photoluminescence spectrum can be used to estimate the quality of nanocrystals formed. The high intensity of green luminescence is indicative of high density of defects and oxygen vacancies, whereas the strong room-temperature UV luminescence indicates that the nanocrystals formed are highly pure and free of defects.

7. Fabrication of doped nanoparticles

In the case of laser ablation of a combined Zn – Ag target immersed in a cell with distilled water, with a laser beam focused at the interface between the two metals, the spectrum of the obtained solution does not exhibit a pronounced maximum, corresponding to single-metal silver particles (Fig. 16).

Silver-doped composite ZnO structures are most likely to be formed in this case. Some research teams [67, 70] reported about obtaining p-type ZnO using silver as an acceptor. As can be seen in Fig. 16, doped ZnO : Ag particles exhibit a significant decrease in the slope of spectral absorptance at the fundamental absorption edge in comparison with undoped ZnO. The band gap of the ZnO : Ag samples is narrower than E_g of undoped ZnO (3.37 eV).

Thus, one can successfully apply laser ablation to form ZnO nanocrystals, whose composition, structure, and optical properties can be changed by varying the experimental conditions.

8. Laser ablation of gadolinium

Lanthanides and their alloys are promising magnetic materials for a number of technological and biomedical applications [71]. In particular, gadolinium and its compounds are used as contrast materials in magnetic resonance tomography as a therapeutic agent for hyperthermia of tumours and as drug carriers. Gadolinium is a ferromagnet with a large magnetic moment. In addition, Gd and its compounds exhibit a strong magnetocaloric effect (MCE), and the temperature of magnetic phase transition in them is close to human body temperature [72, 73]. The problem of forming magnetic nanoparticles with a Curie temperature close to human body temperature, which can be heated to 43 – 45 °C, is extremely urgent for developing controlled local hyperthermia. Preparations based on such materials can ensure temperature self-regulation, because above the Curie temperature a magnetic nanoparticle cannot be heated by an external electromagnetic field. Alloys of 3d and noble metals (rhodium, palladium, and platinum) and alloys and/or intermetallic compounds based on rare earth metals, for example, gadolinium – silicon Gd_5Si_4 (with a maximum MCE temperature $\Delta T = 8.8$ K at $T = 336$ K and magnetic field $H =$ 5 T); gadolinium – silicon – germanium $Gd_5Si_{2.06}Ge_{1.94}$ ($\Delta T = 8$ K at $T = 306$ K and $H = 5$ T); gadolinium–palladium Gd_7Pd_3 ($\Delta T = 8.5$ K at $T = 323$ K and $H =$ 5 T), etc. can be used as magnetic materials. Magnetic measurements revealed that the temperatures of magnetic phase transitions in alloys and compounds of rare earth metals depend strongly on the concentrations of alloyed elements. Varying the content of a certain element in alloy, one can obtain the necessary MCE and provide the required temperature of the magnetic phase transition.

Particles of gadolinium oxide doped with Tb, Eu, Dy, etc. ions can be used as effective luminescent labels in bioanalysis due to their optical properties (sharp emission spectra, long luminescence lifetime), as well as photostability and possibility of inexpensive synthesis.

To be used in biomedical applications, particles, along with all other necessary properties, must be stable in water and/or physiological solutions. This requirement can sometimes be satisfied using nanoparticles with a biocompatible shell. The advantages of nanoparticles are related to the possibility of size-dependent modification of their structural and magnetic properties [74]. For example, nanoscale (subdomain) particles are more promising for magnetic hyperthermia than submicron (multidomain) particles due to the higher efficiency of heating the former in ultimate allowable magnetic fields [75].

In view of the above considerations, it is of interest to analyse the possibility of using laser ablation in liquids to synthesise gadolinium and gadolinium-containing particles and determine the composition and sizes of the particles formed.

Gadolinium nanoparticles have been studied very little, mainly because of extraordinary high sensitivity of Gd to oxidation. As far as we know, there are only few reports on forming gadolinium nanoparticles from the vapour phase or by chemical methods [76, 77]. Most works were devoted to the synthesis of gadolinium oxide nanoparticles doped with rare earth ions [78–80].

The possibility of using laser ablation in liquids to obtain stable Gd nanoparticles was investigated for the first time in [50]. The experiments were performed using a pulsed Nd:YAG laser operating at the first harmonic (1064 nm), with an energy per pulse of 50 mJ and pulse duration of 12 ns. A metallic gadolinium target was fixed on a mobile holder on the bottom of a vessel filled with a liquid (ethanol, water, acetone). The laser radiation was focused on the target surface into a spot with an laser fluence of about 40 J cm^{-2}. An erosion plume was observed near the gadolinium target surface under laser ablation in liquid. The plume luminescence intensity was determined by the laser pulse energy. Several minutes after the irradiation onset, the solution became grey, and a colloidal solution was formed.

Micrographs of the nanoparticles obtained by laser ablation of gadolinium in water and ethanol are shown in Fig. 17. It can be seen that spherical particles with an average size from 10 to 12 nm (ablation in water) and from 6 to 10 nm (ablation in ethanol) are dominant. The size distribution of the particles formed in ethanol is narrower than that for the particles formed in water.

The EDX analysis was used to determine the composition of the nanoparticles formed. The spectra of the samples obtained by laser ablation in ethanol contain gadolinium and carbon lines. Hence, we can suggest that these nanoparticles consist of either gadolinium carbide or have a carbon shell. Indeed, ethyl alcohol can be thermally decomposed during ablation in the plasma plume, and the formed carbon may react with gadolinium to produce carbide GdC_2. In addition, free carbon is likely to form and then cover gadolinium particles, thus preventing them from oxidation.

In the case of laser ablation in distilled water, the EDX spectra contain only gadolinium and oxygen lines (in a ratio close to the stoichiometric ratio for the Gd_2O_3 oxide phase). Similar results were obtained by X-ray diffraction, which showed that laser ablation of metallic gadolinium in distilled water leads to the formation of nanocrystalline gadolinium oxide particles in the monoclinic phase with the lattice constants $a = 14.095$ nm, $b = 3.576$ nm, and $c = 8.769$ nm. No other phases were found [50].

Similar XRD patterns for the powder obtained in ethanol demonstrated a more complex phase composition. This powder was a mixture of gadolinium carbide GdC_2 and gadolinium hydride GdH_3; reflections of metallic Gd were also recorded. Some reflections against a wide background (which is likely to be due to the amorphous phase) in the XRD pattern were not identified. Note that these unidentified peaks could not be attributed to oxide phases, despite the fact that metallic gadolinium is very sensitive to oxidation. It is most likely that some other carbide phases were formed in this case, as well as carbon-coated Gd–GdC_2 nanoparticles.

Laser ablation of a gadolinium target containing 3.5 % terbium in water yielded gadolinium oxide nanocrystals doped with terbium ions, which have luminescent properties. The luminescence spectra of these nanocrystals contain several single peaks (the strongest is at 545 nm), which are due to the electronic transitions of Tb^{3+} in the Gd_2O_3 lattice (Fig. 18).

In the case of single-pulse laser ablation of a combined gadolinium–silicon target in ethanol, Gd and Si particles were formed, which was confirmed by the XRD data (Fig. 19). According to the semiquantitative analysis, the

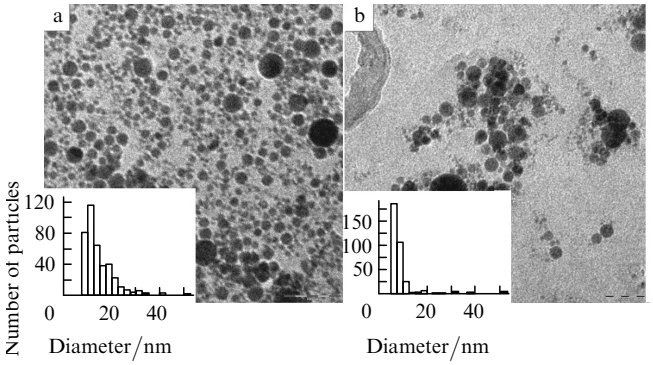

Figure 17. Micrographs and distribution histograms for the nanoparticles obtained by laser ablation (1064 nm) of a gadolinium target in (a) distilled water and (b) ethanol.

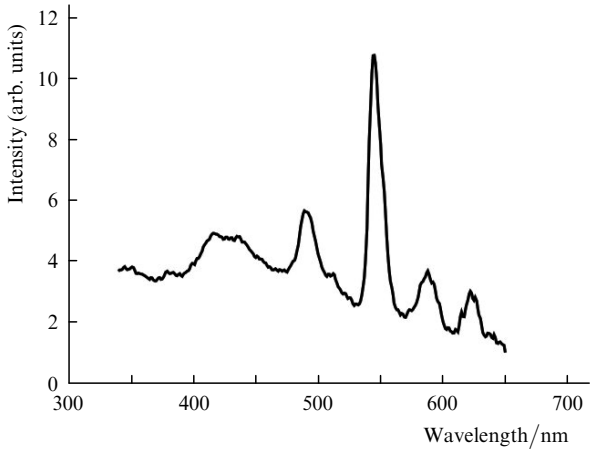

Figure 18. Luminescence spectrum of the nanoparticles formed by laser ablation of a gadolinium target with 3.5 % terbium in water. Luminescence was excited at a wavelength of 276 nm.

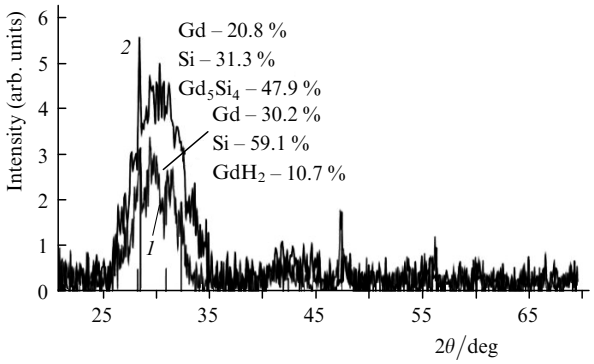

Figure 19. Diffraction patterns of the nanoparticles obtained by (*1*) single-pulse and (*2*) double-pulse laser ablation of a combined Gd–Si target in ethanol.

powder synthesised contained 30.2 vol % hexagonal Gd phase, 59.1 vol % Si, and 10.7 vol % cubic GdH_2 phase.

It is noteworthy that an analysis of the diffraction pattern of the powder obtained by double-pulse ablation of combined Gd–Si target in ethanol revealed a new phase: Gd_5Si_4.

The formation of composite Gd–Si particles under double-pulse laser ablation is likely to be related to the better conditions for mixing ablation product in this regime in comparison with single-pulse ablation. This question needs further study.

9. Laser modification of nanoparticles in solutions

Because the properties of nanoparticles depend on their size and shape [81], the final purpose is to synthesise monodisperse particles with specified parameters. This problem can be solved using additional irradiation of synthesised particles by laser pulses of sufficiently high intensity [34, 82–86]. Currently, the interaction of laser radiation with nanostructures is intensively investigated to develop methods for deliberately changing the nanoparticle structure and morphology [35, 41, 48, 82–88]. It was demonstrated that laser radiation can be used to fragment gold and silver nanoparticles [48, 82, 84] and aggregate them [44, 89]. Laser-induced transformation of nanowires into nanospheres [32] or, vice versa, spherical particles into nanowires [83] was also observed.

Laser irradiation may change not only the morphology of particles but also their composition and structure. In particular, internal segregation of brass nanoparticles and formation of alloy nanoparticles under laser irradiation of a mixture were reported in [39, 90]. Laser-induced internal diffusion in Au–Ag nanoparticles with a core–shell structure was observed in [42]. Because of the selectivity of light absorption by particles, the efficiency of laser-induced modification depends on the laser wavelength; the maximum effect is observed at frequencies of surface plasmon resonances.

In our experiments [36] the silver colloids prepared by PLAL consisted of almost spherical particles with diameters from 15 to 40 nm (Fig. 20a). Laser irradiation of the solutions at a wavelength of 532 nm with an laser fluence above 40 mJ cm^{-2} changed the particle size. After the irradiation the particle diameter did not exceed 15 nm; with an increase in the laser fluence the fragmented particles decreased even more.

The absorption spectra of nanoparticles also changed after irradiation (Fig. 20c). The plasmon resonance band narrowed with a simultaneous increase in the absorption in maximum. These spectral features became more and more pronounced with an increase in the laser fluence from 0.04 to 0.4 J cm^{-2}. The observed narrowing of the plasmon band can be due to the particle size redistribution (with a decrease in the size variance), and the increase in its intensity is most likely to be caused by the increase in the particle concentration in the solution.

The situation was different when the initial particles were agglomerates. In this case, laser irradiation transformed the initial particles into nanowires with an average diameter of about 100 nm and a length up to 600 nm [36]. The shape of the particles after laser-induced modification depends on the irradiation conditions and the character of perturbation relaxation during particle–environment interaction. The mechanisms of interaction of laser radiation with nanoparticles and the corresponding changes are still to be clarified. Therefore, an important condition for optimising the laser-induced modification is to establish the contributions of different physical factors (heating,

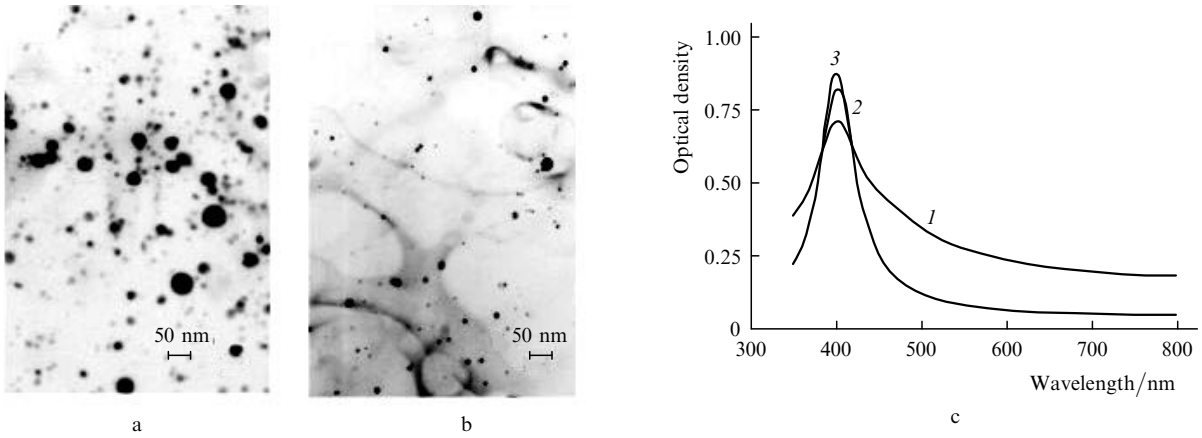

Figure 20. (a, b) Silver nanoparticles and (c) their absorption spectra (a, *1*) before and (b; *2*, *3*) after 5-min exposure of the colloidal solution to 532-nm laser radiation with laser fluences of (*2*) 150 and (*3*) 400 mJ cm^{-2}.

melting, evaporation, laser-induced charging of particles, and particle photofragmentation and aggregation).

When a colloidal solution is laser-irradiated, the radiation is absorbed by nanoparticles (the liquid solvent is generally transparent for laser radiation). As a result, the particles can be heated to the melting and even boiling temperature, and their morphology may change. The possibility of reaching such temperatures depends on the laser fluence, pulse duration, irradiation time, etc. [91, 92].

In our experiments the possibility of heating silver particles to the melting and evaporation temperatures was confirmed by calculations of the nanoparticle temperature, based on measuring the absorbed laser energy. The temperature of silver particles was estimated from the balance between the absorbed laser energy and the thermal loss during the heat exchange with the surrounding liquid. The calculations showed that the nanoparticle temperature exceeds the melting point of silver at laser fluences above 50 mJ cm^{-2} and reaches the boiling point at about 100 mJ cm^{-2} [36]. If the laser radiation density is low and the nanoparticle temperature does not reach the melting point, the particles do not change in shape and size. However, if the nanoparticle temperature is above the melting temperature but below the boiling point, it is only the particle shape that changes. The particles change in both shape and size only when heated to the boiling temperature.

Other possible mechanism of nanoparticle modification in the solution was discussed in [91, 92]. Due to the thermal conductivity, the absorbed laser energy is transferred to the surrounding liquid; therefore, a nanoparticle is surrounded by a vapour shell for some time after the laser pulse. At the initial stage, the vapour pressure in the shell is close to the saturated vapour pressure of the liquid at the melting temperature of the nanoparticle material (about 10^3 K for Au, Ag, and Cu). The interaction of molten nanoparticles with high-pressure vapour may lead to their fragmentation, for example, because of the asymmetry of the vapour cloud [92].

Decomposition of particles due to their charging as a result of photoelectron emission [93] can be efficient under UV laser excitation, when the photon energy exceeds the electron work function of the metal. In particular, the mechanism of Coulomb breakup of molten particles was considered in [93] by the example of silver nanoparticles exposed to 266-nm laser radiation.

For gold nanoparticles heating effects were found to be decisive under laser irradiation at $\lambda = 532$ nm [94]. Exposure of nanoparticles to laser radiation with a wavelength lying in the range of plasma resonance leads generally to a decrease in the particle size as a result of light absorption by particles and their partial evaporation.

Figure 21 shows typical optical absorption spectra of gold nanoparticles obtained by ablation of a metal target in ethanol using the second harmonic of yttrium aluminium laser (pulse duration, 15 ns; laser fluence, 5 J cm^{-2}) and then laser-irradiated in the absence of target for 3 min at wavelengths of 532 and 266 nm, with laser fluences of 0.3 and 0.1 J cm^{-2}, respectively. As can be seen in the figure, the absorption maximum is blue-shifted (from 528 to 519 nm for irradiation at $\lambda = 532$ nm and to 517 nm for $\lambda = 266$ nm).

In accordance with the Mie theory, which describes the optical properties of small metal particles, the observed shift

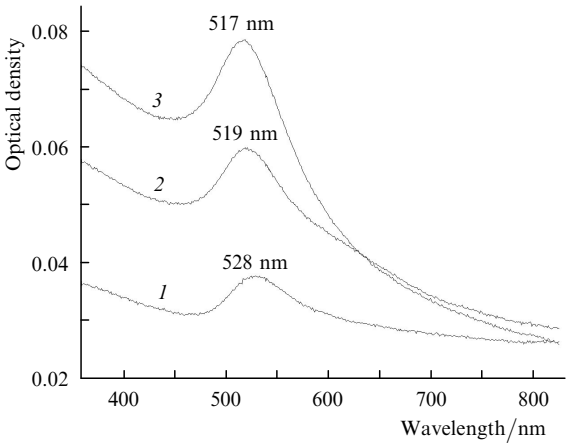

Figure 21. Optical absorption spectra of gold nanoparticles (*1*) before and (*2*) after 3-min laser irradiation at wavelengths of (*2*) 532 and (*3*) 266 nm.

of the absorption maximum indicates that the additional laser irradiation of the colloidal solution reduces the average particle size [31]. Larger particles, which absorb a significant part of laser radiation because of their larger absorption cross section, are the first to be fragmented. After the laser irradiation, the UV absorption of the solution increased, which corresponded to a higher concentration of Au atoms in it. The change in the absorption after the laser irradiation indicates that the total concentration of Au particles in the solution also increases. At the same time, the narrowing of the red tail of plasmon resonance band can be related to a decrease in the concentration of aggregated particles [82].

The TEM images of the samples before and after laser irradiation confirm the suggestion about particle fragmentation, which was based on the analysis of the absorption spectra. After additional irradiation relatively large (15–20 nm) particles decrease in size to 2.5–5 nm.

Note that laser irradiation of metal colloids may cause not only fragmentation but also fusion of particles due to their photothermal alloying [83, 95]. The type of the solvent (stabiliser) determines to a great extent the scenario according to which laser-stimulated modification occurs [86].

Figure 22 presents micrographs of gold nanoparticles obtained by laser ablation in an aqueous solution of fructose with a concentration of 0.14 mol L^{-1} before and after additional laser irradiation at $\lambda = 532$ nm with an laser fluence of 0.3 J cm^{-2}. One can see that the irradiation leads to the formation of agglomerates composed of many closely contacting small nanoparticles.

The optical spectra of bimetallic Ag–Cu particles also turned out to be sensitive to additional laser irradiation. The additional irradiation of colloidal solutions by the second harmonic of Nd:YAG laser (532 nm, 350 mJ cm^{-2}) leads to a relative increase in absorption in the range of 500–580 nm and reduces absorption for wavelengths below 500 nm (Fig. 23). The maximum absorption in the range of plasmon resonance decreases, and the absorption peak is red-shifted toward the absorption maximum for copper. In addition, the absorption band is broadened, as can clearly be seen for the normalised absorption spectra. The changes in the absorption spectra indicate a further change in the structure and/or morphology of bimetallic particles as a result of laser irradiation.

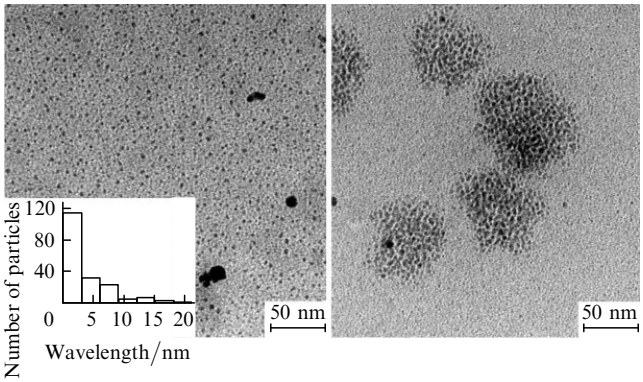

Figure 22. TEM images of gold nanoparticles obtained by laser ablation in an aqueous solution of fructose with a concentration of 0.14 mol L^{-1} before (left) and after (right) additional laser irradiation with a wavelength of 532 nm and laser fluence of 0.3 J cm^{-2}. The initial colloid contains spherical particles 3–5 nm in diameter.

Note that these changes differ from the changes in the absorption spectra of a mixture of single-metal silver and copper particles subjected to additional irradiation by the second harmonic of yttrium aluminium laser (with 400 mJ cm^{-2}). The initial colloids were prepared by laser ablation (1064 nm) of the corresponding metal targets in ethanol. Two individual peaks, corresponding to the plasmon bands of each metal, are observed for the mixture of single-metal particles before the irradiation. The irradiated mixtures are characterised by wide absorption spectra with a maximum in the range of 550 – 560 nm. Note that the laser-induced spectral changes depend on the irradiation time. The intermediate absorption spectra of colloidal solution correspond to the intermediate structures of complex shape, formed by contacting nanoparticles. A similar transformation of the spectra of mixtures of Ag and Cu colloids under laser irradiation was observed by Shafeev et al. [90]. The experimental results showed that the final Ag – Cu particles had rather a mixed alloy structure than the core – shell structure, although silver and copper cannot form solid solutions at room temperature.

The absorption spectra of irradiated bimetallic Ag – Cu nanoparticles indicate that formation of hybrid particles with the dominant copper content is most likely to occur [96]. Similarly, laser irradiation of brass nanoparticles (60 % Cu, 40 % Zn) in ethanol caused zinc diffusion to the particle periphery and gradual displacement of the plasmon resonance of brass nanoparticles to that for copper nanoparticles [39, 92]. It was suggested that brass nanoparticles lose zinc as a result of irradiation, which apparently passes to the solution in the form of oxide or hydroxide. The internal segregation of small composite nanoparticles subjected to laser irradiation was explained by the effect of high pressure, which modified the phase diagram of the composite particles (the component with a lower melting temperature should be displaced to the particle periphery).

The method of laser-induced modification of a mixture of individual colloids is expected to be applied to other materials. In particular, our recent experiments showed that laser irradiation of a mixture of the Gd and Si colloids, prepared by laser ablation in ethanol, leads to the formation of the Gd_5Si_4 phase [97], while laser irradiation of a mixture of ZnO and Ag particles facilitates formation of doped zinc oxide structures.

10. Conclusions

We reviewed the studies devoted to the formation and modification of nanoparticles by laser ablation of solid targets in liquids. The results of applying single and double laser pulses are summarised. The optimal characteristics of laser pulses and schemes of mutual configuration of light beams for forming bimetallic nanoparticles (by the example of Ag – Cu and Ag – Au particles), luminescent zinc oxide particles, and magnetic gadolinium-containing particles are found.

It is demonstrated that laser ablation in liquids is an effective and universal tool for synthesising nanoparticles of different compositions. It has a certain flexibility in controlling their properties with a corresponding choice of laser parameters and liquid type, in particular, by combining different solid targets and liquids to obtain nanostructures

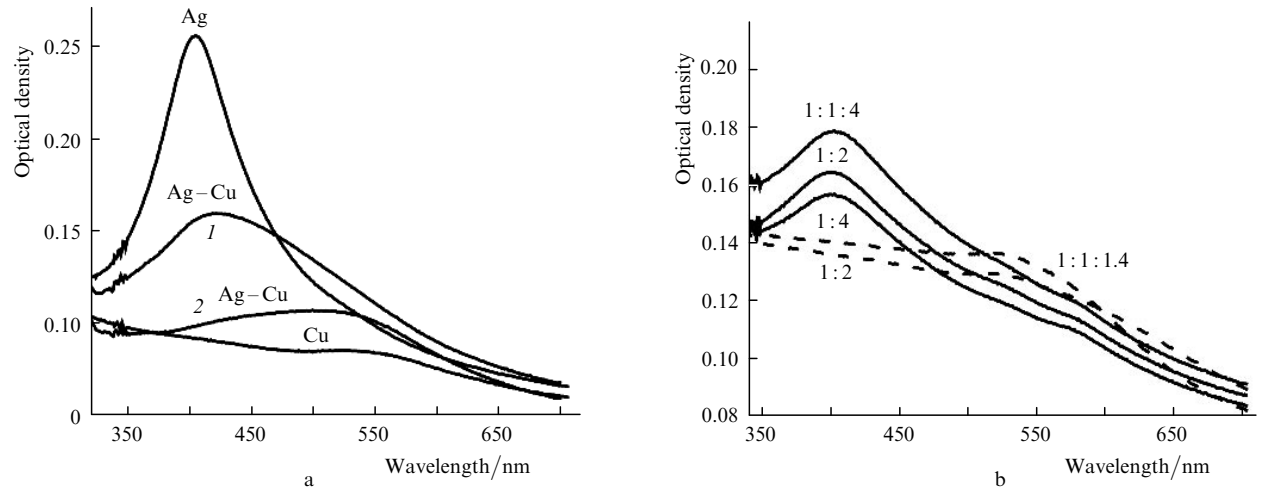

Figure 23. Absorption spectra of the (a) colloidal solutions of bimetallic Ag – Cu nanoparticles (the spectra of individual silver and copper colloids are denoted as Ag and Cu) in the initial state (*1*) and after irradiation by the second harmonic of Nd^{3+} : YAG laser (*2*) and (b) a mixture single-metal silver and copper particles before (solid lines) and after (dashed lines) additional irradiation by the second harmonic of yttrium aluminium laser ($\lambda = 532$ nm, 400 mJ cm^{-2}).

of new composition (for example, immiscible alloys and metastable phases).

It is shown that laser-induced effects in metal and composite particles can be used for selective modification of their morphology and internal structure.

According to the experimental and theoretical data, the characteristics of synthesised nanoparticles depend on the properties of the laser plasma, in particular, the density of its different components. Having understood the properties of laser plasma evolution, one can optimise more efficiently the synthesis conditions. In this context, the time-resolved methods of optical emission spectroscopy and image detection can provide data that are important for identifying the composition of laser plasma and monitoring its evolution.

Laser synthesis and modification of nanoparticles in liquids is relatively young but rapidly developing field of research, which has a wide range of practical applications. Currently, nanoparticles are used to improve physical and chemical properties of various composites. New applications are expected in medicine, electronics, catalysis, optics, and biophotonics.

Acknowledgements. This review was prepared within the joint Russian – Belarusian project (Belarusian Foundation for Fundamental Research – Russian Foundation for Basic Research, Grant No. F10R-115).

References

1. Shafeev G.A. *Lasers in Chemistry 2* (Wienheim: Wiley VCH Verlag GmbH&Co, KGaA, 2008) pp 713 – 741.
2. Kabashin A.V., Meunier M. *Recent Advances in Laser Processing of Advanced Materials* (Oxford: Elsevier, 2006) pp 1 – 36.
3. Yang G.W. *Prog. Mater. Sci.*, **52**, 648 (2007).
4. Wang A.Q., Liu J.-H., Linb S.D., Lin T.-S., Mou C.-Y. *J. Catalysis*, **233**, 186 (2005).
5. Bogaerts A., Chen Zh., Gijbels R., Vertes A. *Spectrochim. Acta B*, **58**, 1867 (2003).
6. Amans D., Chenus A-C., Ledoux G., Dujardin C., Reynaud C., Sublemontier O., Masenelli-Varlot K., Guillos O. *Diamond & Related Mater.*, **18**, 177 (2009).
7. Morales A.M., Lieber C.M. *Science*, **279**, 208 (1998).
8. Tsuji T., Toshihiko K., Hamagami T., Kawamura T., Yamaki J., Tsuji M. *Chem. Lett.*, **33**, 1136 (2004).
9. Patil P.P., Phase D.M., Kulkarni S.A., Ghaisas S.V., Kulkarni S.K., Kanrtkar S.M., et al. *Phys. Rev. Lett.*, **58**, 238 (1987).
10. De Giacomo A., Dell'Aglio M., De Pascale O. *Appl. Phys. A*, **79**, 1035 (2004).
11. De Giacomo A., Dell'Aglio M., De Pascale O., Capitelli M. *Spectrochim. Acta B*, **62**, 721 (2007).
12. Sakka T., Iwanaga S., Ogata Y.H., Matsunawa A., Takemoto T. *J. Chem. Phys.*, **112**, 8645 (2000).
13. Sakka T., Takatani K., Ogata Y.H., Mabuchi M. *J. Phys. D: Appl. Phys.*, **35**, 65 (2002).
14. Brennen C.E. *Cavitation and Bubble Dynamics* (Oxford: Oxford University Press, 1995).
15. De Giacomo A., Dell'Aglio M., Colao F., Fantoni R. *Spectrochim. Acta B*, **59**, 1431 (2004).
16. Pichahchy A.E, Cremers D.A., Ferris M.J. *Spectrochim. Acta B*, **52**, 25 (1997).
17. Nevar E.A., Savastenko N.A., Bryuzer V., Lopatik D.A., May F., Butsen A.V., Tarasenko N.V., Burakov B.C. *Zh. Prikl. Spektrosk.* **77**, 136 (2010).
18. Nakamura S., Ito Y., Sone K. *Anal. Chem.*, **68**, 2981 (1996).
19. Lazic V., Colao F., Fantoni R., Spizzichino V. *Spectrochim. Acta B*, **60**, 1002 (2005).
20. Lazic V., Colao F., Fantoni R., Spizzichino V. *Spectrochim. Acta B*, **60**, 1014 (2005).
21. Sakka T., Oguchi H., Ogata Y.H. *J. Phys. Conf. Ser.*, **59**, 559 (2007).
22. Sakka T., Yamagata H., Oguchi H., Fukami K., Ogata Y.H. *Appl. Surf. Sci.*, **255**, 9576 (2009).
23. Burakov V.S., Tarasenko N.V., Butsen A.V., Rozantsev V.A., Nedel'ko M.I. *Eur. Phys. J. Appl. Phys.*, **30**, 107 (2005).
24. Burakov B.C., Butsen A.V., Tarasenko N.V. *Izv. Vyssh. Uchebn. Zaved., Ser. Priborostroenie*, **49**, 146 (2006).
25. Arepalli S., Scott C.D. *Chem. Phys. Lett.*, **302**, 139 (1999).
26. Guo T., Nikolaev P., Thess A., Colbert D.T., Smalley R.E. *Chem. Phys. Lett.*, **243**, 49 (1995).
27. Burakov V.S., Tarasenko N.V., Nedel'ko M.I., Isakov S.N. *Spectrochim. Acta B*, **63**, 19 (2008).
28. Sakka T., Saito K., Ogata Y.H. *J. Appl. Phys.*, **97**, 014902 (2005).
29. Liang C.H., Shimizu Y., Sasaki T., Koshizaki N. *Appl. Phys. A*, **80**, 819 (2005).
30. Burakov B.C., Butsen A.V., Tarasenko N.V. *Zh. Prikl. Spektrosk.*, **77** (3), 416 (2010).
31. Boren C.F., Huffman D.R. *Absorption and Scattering of Light by Small Particles* (New York: Wiley, 1983).
32. Link S., Burda C., Nikoobakht B., El-Sayed M.A. *J. Phys. Chem. B*, **104**, 6152 (2000).
33. Kreibig U., Vollmer M. *Optical Properties of Metal Clusters* (Berlin: Springer, 1995).
34. Gonzalo J., Babonneau D., Afonso C.N., Barnes J.-P. *J. Appl. Phys.*, **96**, 5163 (2000).
35. Butsen A.V., Nevar E.A. *Vestsi NAN Belarusi*, **5**, 94 (2006).
36. Callegari A., Tonti D., Cheggui M. *Nanoletters*, **3**, 1565 (2003).
37. Kawasaki M., Nishimura N. *Appl. Surf. Sci.*, **253**, 2208 (2006).
38. Lee I., Han S.W., Kim K. *Chem. Commun.*, **18**, 1782 (2001).
39. Voronov V.V., Kazakevich P.V., Simakin A.V., Shafeev G.A. *Kvantovaya Elektron.*, **34**, 951 (2004) [*Quantum Electron.*, **34**, 951 (2004)].
40. Poondi D., Dobbins T., Singh J. *J. Mater. Sci.*, **35**, 6237 (2000).
41. Compagnini G., Messina E., Puglisi O., Nicolosi V. *Appl. Surf. Sci.*, **254**, 1007 (2007).
42. Hodak J.H., Henglein A., Giersig M. *J. Phys. Chem. B*, **104**, 11708 (2000).

43. Chen Y.-H., Yeh C.-S. *Chem. Commun.*, **4**, 371 (2001).
44. Kamat P.V. *J. Phys. Chem. B*, **106**, 7729 (2002).
45. Zeng H.B., Cai W.P., Li Y. *J. Phys. Chem. B*, **109**, 18260 (2005).
46. Liang C.Y., Shimizu T., Sasaki N., Koshizaki M. *J. Phys. Chem. B*, **107**, 9220 (2003).
47. Bajaj G., Soni R.K. *J. Nanopart. Res.*, **12**, 2597 (2010).
48. Henglein A. *J. Phys. Chem.*, **97**, 5457 (1993).
49. Bokshits Yu.V., Shevchenko G.P., Sviridov V.V. *Vestsi NAN Belarusi, Ser. Khim. Navuk*, **1**, 19 (2001).
50. Tarasenko N.V., Butsen A.V., Nevar A.A. *Appl. Phys. A*, **93**, 837 (2008).
51. Sasaki K., Nakamuta Y., Hirajima T., Tuovinen O.H. *Hydrometallurgy*, **95**, 153 (2009).
52. Rath R.K., Subramanian S., Sivanandam V., Pradeep T. *Can. Metal. Quart.*, **40** (1), 1 (2001).
53. Anikin K.V., Melnik N.N., Simakin A.V., et al. *Chem. Phys. Lett.*, **366**, 357 (2002).
54. Li Y., Xu G., Zhu Y.L., Ma X.L., Cheng H.M. *Sol. State Commun.*, **142**, 441 (2007).
55. Usui H., Shimizu Y., Sasaki T. *J. Phys. Chem. B*, **109**, 120 (2005).
56. He C., Sasaki T., Usui H., Shimizu Y., Koshizaki N. *J. Photochem. Photobiol A: Chemistry*, **191**, 66 (2007).
57. He C., Sasaki T., Shimizu Y., Koshizaki N. *Appl. Surf. Sci.,* **254**, 2196 (2008).
58. Singh S.C., Gopal R. *Phys. E: Low-Dimensional Syst. Nanostruct.*, **40**, 724 (2008).
59. Thareja R.K., Shukla S. *Appl. Surf. Sci.*, **253**, 8889 (2007).
60. Fan Z., Lu J.G. *J. Nanosci. Nanotechnol.*, **5**, 1561 (2005).
61. Özgür Ü., Alilov Y.I., Liu C. *J. Appl. Phys.*, **98**, 041301 (2005).
62. Klingshirn C. *Phys. Stat. Sol. B*, **244**, 3027 (2007).
63. Pearton S.J., Norton D.P., Ip K., Heo Y.W., Steiner T. *Prog. Mater. Sci.*, **50**, 293 (2005).
64. Rakhshani A.E., Kokaj J., Mathew J., Peradeep B. *App. Phys. A*, **86**, 377 (2007).
65. Labuayai S., Promarak V., Maensiri S. *Appl. Phys. A*, **94**, 755 (2009).
66. Zherikhin A.N., Khudobenko A.I., Vil'yams R.T., Vilkinson D., User K.B., Hiong G., Voronov V.V. *Kvantovaya Elektron.*, **33** (11), 975 (2003) [*Quantum Electron.*, **33** (11), 975 (2003)].
67. Zhao S., Zhou Y., Zhao K., Liu Z., Han P., Wang S., Xiang W., Chen Z., Lü H., Cheng B., Yang G. *Phys. B*, **373**, 154 (2006).
68. Djurisic A.B., Leung Y.H., Tam K.H., Hsu Y.F., Ding L., Ge W.K., Zhong Y.C., Wong K.S., Chan W.K., Tam H.L., Cheah K.W., Kwok W.M., Phillips D.L. *Nanotechnol.*, **18**, 095702 (2007).
69. Ozerov I., Arab M., Safarov V.I. *Appl. Surf. Sci.*, **226**, 242 (2004).
70. Song Y-W., Kim K., Lee S.Y. *Thin Sol. Films*, **518** (4), 1318 (2009).
71. Bohigas X., Molins E., Roig A., Tegada J., Zhang X.X. *IEEE Trans. Magn.*, **36**, 538 (2000).
72. Giguere A., Foldeaki M., Gopal B.R., Chahine R., Bose T.K., Frydman A., Barclay J.A. *Phys. Rev. Lett.*, **83**, 2262 (1999).
73. Tishin A.M., Spichkin Yu.I. *Magnetocaloric Effect and its Application* (Bristol – Philadelphia: Inst. Phys. Publ., 2003).
74. Wickham J.N., Herhold A.B., Alivisatos A.P. *Phys. Rev. Lett.*, **84**, 923 (2000).
75. Tartaj P., Morales M.P. *J. Phys. D: Appl. Phys.*, **36**, R182 (2003).
76. Aruna I., Mehta B.R., Malhotra L.K., Shivaprasad S.M. *Adv. Func. Mater.*, **15**, 131 (2005).
77. Si P.Z., Skorvanek I., Kovac J., Geng D.Y., Zhao X.G., Zhang Z.D. *J. Appl. Phys.*, **94**, 6779 (2003).
78. Dosev D., Nichkova M., Liu M., Guo B., Liu G.-Y., Hammock B.D., Kennedy I.M. *J. Biomed. Opt.*, **10** (6), 064006 (2005).
79. Gogdon W.O., Carter J.A., Tissue B.M. *J. Luminesc.*, **108**, 339 (2004).
80. Ledoux G., Amans D., Dujardin C., Masenelli-Varlot M. *Nanotechnol.*, **20** (44), 445605 (2009).
81. Link S., El Sayed M.A. *Int. Rev. Phys. Chem.*, **19** (3), 409 (2000).
82. Mafuné F., Kohno J., Takeda Y., Kondow T., Sawabe H. *J. Phys. Chem. B*, **106** (34), 8555 (2002).
83. Tsuji T., Okazaki Y., Higuchi T., Tsuji M. *Appl. Surf. Sci.*, **211**, 189 (2003).
84. Takami A., Kurita H., Koda S. *J. Phys. Chem. B*, **103** (8), 1226 (1999).
85. Sugiyama M., Okazaki H., Koda S. *Jpn. J. Appl. Phys.*, **41** (7A), 4666 (2002).
86. Sun F., Cai W., Li Y., Duan G., Nichols W.T., Liang C., Koshizaki N., Fang Q., Boyd I.W. *Appl. Phys. B*, **81**, 765 (2005).
87. Tarasenko N.V., Butsen A.V., Nevar E.A., Savastenko N.A. *Appl. Surf. Sci.*, **252**, 4439 (2006).
88. Izgaliev A.T., Simakin A.V., Shafeev P.A. *Kvantovaya Elektron.*, **34** (1), 47 (2004) [*Quantum Electron.*, **34** (1), 47 (2004)].
89. Burda C. *Optical Spectroscopy of Nanophase Material*. Ed. by Zhong Lin Wang (Weinheim: Wiley-VCH Verlag GmbH, 2000) p. 197.
90. Kazakevich P.V., Simakin A.V., Voronov V.V., Shafeev G.A. *Appl. Surf. Sci.*, **252**, 4373 (2006).
91. Bozon-Verdyura F., Brainer R., Voronov V.V., Kirichenko N.A., Simakin A.V., Shafeev G.A. *Kvantovaya Elektron.,* **33** (8), 714 (2003) [*Quantum Electron.*, **33** (8), 714 (2003)].
92. Simakin A.V., Voronov V.V., Shafeev G.A. *Trudy IOFAN*, **60**, 83 (2004).
93. Kamat P.V., Flumiani M., Hartland G.V. *J. Phys. Chem. B*, **102**, 3123 (1998).
94. Chandrakharan N., Kamat P.V., Hu J., Jones G.J. *Phys. Chem. B*, **104**, 11103 (2000).

95. Aslam M., Gopakumar G., Shoba T.L. *J. Colloid. Inter. Sci.*, **255**, 79 (2002).
96. Tsuji M., Hikino S., Sano Y., Horigome M. *Chem. Lett.*, **38**, 518 (2009).
97. Tarasenko N.V., Butsen A.V., Nedelko M.I., in *Proc. EOS Conf. on Laser Ablation and Nanoparticle Generation in Liquids (ANGEL 2010)* (Switzerland, Engelberg, 2010).